Determination optical properties of tissue-like phantoms using diffuse reflectance and transmittance spectroscopy

Huihui Lu, Jacqueline Gunther, Stefan Andersson-Engels

Huihui Lu, Jacqueline Gunther, Stefan Andersson-Engels, "Determination optical properties of tissue-like phantoms using diffuse reflectance and transmittance spectroscopy ," Proc. SPIE 10820, Optics in Health Care and Biomedical Optics VIII, 108202X (23 October 2018); doi: 10.1117/12.2501183

SPIE.

Event: SPIE/COS Photonics Asia, 2018, Beijing, China

Determination optical properties of tissue-like phantoms using diffuse reflectance and transmittance spectroscopy

Huihui Lu[a], Jacqueline Gunther[a], and Stefan Andersson-Engels[a,b]
[a] Tyndall National Institute, University College Cork, Cork, Ireland; [b] Department of Physics, University College Cork, Cork, Ireland

ABSTRACT

We present a simple, convenient fibre-optics probe system for the determination optical properties of tissue-like liquid phantoms based on diffuse reflectance and transmittance measurements at the wavelength of visible-near-infrared region. The method combined Monte Carlo simulations, multiple polynomial regression and a Newton-Raphson algorithm for solving nonlinear equation system. In the range of optical properties of phantom with the μ_a at 0 – 0.5 cm^{-1} and the μ_s' at 3 – 45 cm^{-1}, the mean prediction error at 630 nm was 1.91 % for μ_s' and 7.51 % for μ_a. The performance of the method is further tested by predictive error and validated using similar matrix of milk-ink phantoms on reflectance and transmittance.

Keywords: Optical properties, Spectroscopy, Fibre-optics, Tissue diagnostics

1. INTRODUCTION

The optical properties for the determination of biological tissue is vital to the development of medical diagnostic devices. The absorption coefficient μ_a may provide the information on the tissue chromophores, whilst scattering coefficient μ_s and anisotropy g may be used to characterize the various scattering components in the tissue. Convenient and accessible methods for measuring optical properties are of extremely useful for research in areas not only for diagnostic purposes, e.g. variation of light absorption in tissue enables to monitor changes in blood oxygenation and concentrations of oxygenated and deoxygenated haemoglobin[1], but also in therapeutic applications, e.g. knowing the optical properties of the tissue is essential for calculating the light dosage delivered to tissue by laser therapy[2].

A variety of techniques used to measure optical properties have been reviewed[3, 4]. A common method is based on integrating sphere set up, which may consist of a single or double integrating spheres[5, 6]. This method acquire spectra from three measurement modes namely collimated transmittance, total transmittance and total diffuse reflectance, followed by the inversion of these measurements using the adding-doubling method. The technique base on diffuse reflectance measurement has a significant potential in medical diagnostics and monitoring as it offers the advantages of non-invasive or minimally invasive measurements. Principles and applications of tissue optical reflectance and transmittance have been comprehensive discussed by Wilson and Jacques[7]. Different instrumental techniques based on diffuse reflectance measurements have been devised, based on time-resolved[8], frequency-domain[9, 10], and continuous wave[11, 12] method. However, these methods require bulky and expensive equipment, and a large sample volume.

In this paper, we present a simple, convenient fibre-optics probe system for the determination of optical properties of tissue-like liquid phantoms based on diffuse reflectance (R) and transmittance (T) spectroscopy measurements. The system collects reflectance and transmittance measurements at the wavelength of visible-near-infrared region simultaneously without moving the sample and is applicable for measurement in small sample volume. To accomplish this a calibration model based on multiple polynomial regression is established with a set of milk-ink phantoms with optical properties within a range typical for biological tissue. Then, the Newton-Raphson algorithm is performed for solving nonlinear equation system and extracting μ_a and μ_s' from diffuse reflectance and transmittance measurements. The performance of the method is further tested by predictive error and validated using similar matrix of milk-ink phantoms on reflectance and transmittance.

Optics in Health Care and Biomedical Optics VIII, edited by Qingming Luo, Xingde Li, Ying Gu, Yuguo Tang, Dan Zhu,
Proc. of SPIE Vol. 10820, 108202X · © 2018 SPIE · CCC code: 0277-786X/18/$18 · doi: 10.1117/12.2501183

2. MATERIALS AND METHODS

2.1 Collimated transmission setup

With the collimated transmission setup the absorption coefficient (μ_a) of India ink (Winsor & Newton® black India ink) and the scattering coefficient (μ_s) of milk (Dawn® low fat milk, produced in Ireland) can be measured with a broad wavelength range. Figure 1 shows a sketch of collimated transmission setup to measure the total attenuation coefficient ($\mu_t = \mu_a + \mu_s$). A halogen lamp (HL-2000, Ocean Optics, B.V, Netherlands), spectrometer (FLAME-S-VIS-NIR-ES, Ocean Optics, B.V, Netherlands) and collimation lens (LA4647, Thorlabs GmbH, Deutschland) were used in this system. The distance between the sample and detector is large enough, in which a small acceptance angel (0.46 ^{0}) was used to minimize the collection of scattered light.

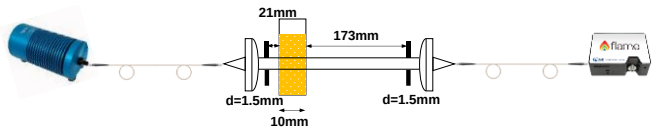

Figure 1. Sketch of collimated transmission setup for measurement of the attenuation coefficient μ_t=μ_a+μ_s.

The total attenuation coefficient μ_t is calculated from the Beer-Lambert law:

$$I(\lambda) = I_0 \times \exp(\mu_t(\lambda) \cdot c \cdot d) \qquad \textbf{(1)}$$

Where *c* is the concentration, *d* is the sample path length, I_0 is the incident intensity and $I(\lambda)$ is the measured intensity.

For solely absorbing samples, $\mu_a \gg \mu_s$, the measured attenuation coefficient equals the absorption coefficient, $\mu_t = \mu_a$. For solely scattering sample, $\mu_s \gg \mu_a$, therefore $\mu_t = \mu_s$, like it is the case for milk dilutions. To avoid the influence of multiple scattered light on the measurement either the sample can diluted or the thickness of the cuvette can be decreased. In this study, the milk were diluted with water to the concentration of less than 5%, which is low enough to avoid the influence of multiple scattered light on the measurement.

We have performed several transmission measurements on different concentrations of ink/milk and a linear fit was made. The absorption coefficient of India ink and the scattering coefficient of low fat milk have been determined by extrapolating absorption/scattering coefficient values obtained in added solution series experiment at low ink/milk concentrations.

2.2 Fibre-optic system setup

Figure 2 shows the schematic view of fiber-optic system setup used for the diffuse reflectance and transmittance measurements. The system consists of a halogen light source (HL-2000, Ocean Optics, B.V, Netherlands), bifurcated fiber optic probe (Thorlabs GmbH, Deutschland), a sample cell and spectrometers (FLAME-S-VIS-NIR-ES, Ocean Optics, B.V, Netherlands) with wavelength grating from 350 – 1000 nm and a laptop computers. The fiber optic probe contained two 1000 µm diameter fibers for light delivery and light collection, respectively, with an outer diameter of 2.1 mm. The center-to-center distance between the source and detector fibers for reflectance is 1065 µm. The cuvette holder was printed by 3D technology which gives the flexibility of phantom sample thickness geometry consideration. The turbid medium samples were placed into the cuvette for the measurements.

The input light power of spectrometer for reflectance measurement was calibrated with input light power of spectrometer for transmittance measurement using water-filled cuvette before turbid medium measurement. To minimize any interference from background light, the dark measurements are recorded prior to the actual measurements and subtracted from the raw data. We collected the total diffuse reflectance and transmittance data of one sample simultaneously using two spectrometers. Reflectance and transmittance were calculated as following equations:

$$R(\%) = \frac{I_r}{I_0'} \qquad \textbf{(2)}$$

$$T(\%) = \frac{I_t}{I_0} \qquad \textbf{(3)}$$

Where I_r is the measured diffuse reflectance intensity, I_t is the measured transmittance intensity, I_0 is the input light power which subtracted the dark measurement, and I_0' is calibrated input light power for reflectance spectroscopy measurement.

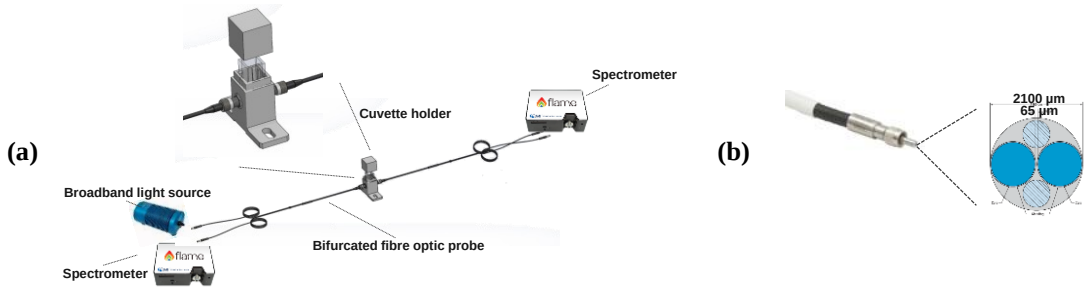

Figure 2. **(a)** Schematic view of fibre-optic system setup for reflectance and transmittance measurement; and **(b)** fibre probe geometry.

2.3 Phantom samples

The scattering and absorption coefficients of the milk and the India ink were determined by the collimated transmission setup described in section 2.1. The obtained scattering / absorption coefficient of the phantoms were derived as a combination of the milk / ink with pure water, each of which was weighted by its concentration in the phantoms. The absorption of pure ink is much higher than that of typical biological substances, therefore the ink were pre-diluted into water solution and we used it as a stock ink-water solution. The absorption coefficients μ_a of the ink dilutions were calculated as 85% of the attenuation coefficients μ_t because 15% of the attenuation could be attributed to scattering by the carbon particles in the original ink solution[13].

In order to carry out the multiple polynomial regression measurements, the liquid phantoms prepared as aqueous mixtures of milk and Indian ink were divided as two groups: A calibration set of a matrix of 7×7 liquid phantoms (forty nine samples) were prepared for building the multiple polynomial regression evaluation and a validation set of similar matrix phantom samples to perform the validation experiments. The liquid phantom set was prepared to cover the range of reduced scattering coefficients at 630 nm with 6, 12, 18, 24, 30, 36, 42 cm^{-1} and absorption coefficient values at 630 nm with 0.01, 0.05, 0.1, 0.2, 0.3, 0.4, 0.5 cm^{-1}.

3. RESULTS AND DISCUSSIONS

3.1 Monte Carlo Simulation and Geometry consideration

To consider the geometry set up of fibre-optics probe system, such as source-detector distance and phantom thickness, we utilized Monte Carlo software[14] to simulate reflectance and transmittance *R(r)* data with various combination of μ_a and μ_s' with ranges typical for biological tissue. Parameters of scattering anisotropy *g* and refraction index *n* were given as 0.7 and 1.38 for the phantoms[7, 15] and were kept fixed in the simulations. The reduced scattering coefficients is $\mu_s' = \mu_s (1-g)$. We used a semi-infinite slab with three bulk layers, the slab was placed between semi-infinite glass slides with thickness of d_{glass} = 1.2 mm and refractive index n_{glass} = 1.52. In each simulation, 10^7 photons were injected. All numerical analysis and algorithm in this paper were created with Matlab 2016a (The MathWorks Inc. Natick, Massachusetts).

Figure 3 shows MCML reflectance and transmittance simulated *R(r)* data with different phantom thickness at 1, 2, 5, 10 mm. The thickness selected for simulation is based on the commercial availability of different pathlength cuvettes. It is clearly observed that the transmittance *R(r)* data for various combination of μ_a and μ_s' of liquid phantoms span a wider range with phantoms thickness increases, which indicates that the optical properties may be determined with better accuracy with 5 or 10 mm phantom thickness. It is also noted that phantoms with μ_a at 1 cm^{-1} and μ_s' at 45 cm^{-1} with 10 mm thickness gave more noise and much lower signal of transmittance than that with 5 mm. Therefore, 5 mm phantom thickness was selected for further investigation.

In figure 4(a), μ_s' is kept constant at values of 3 and 45 cm^{-1}, respectively, while μ_a varied within the range from 0.01 – 1 cm^{-1}. It appears that changes of μ_a have a negligible effect on reflectance at distance close to the source, but have effect on transmittance at μ_s' value of 45 cm^{-1}. In figure 4(b), μ_a is kept constant at values of 0.01 and 1 cm^{-1}, respectively, whereas

μ_s' varied within the range from 3 – 45 cm^{-1}. It is notable that there is little variation in a pivot point region (between *R(r)* 2 mm or 6 mm) on reflectance. This indicates that μ_s' may be determined with good accuracy from close distance. Hence, the bifurcated fiber optic probe contained two 1000 µm diameter fibres for light delivery and light collection matching this source-detector separation was selected. The centre-to-centre distance between the source and detector fibres for reflectance is 1065 µm.

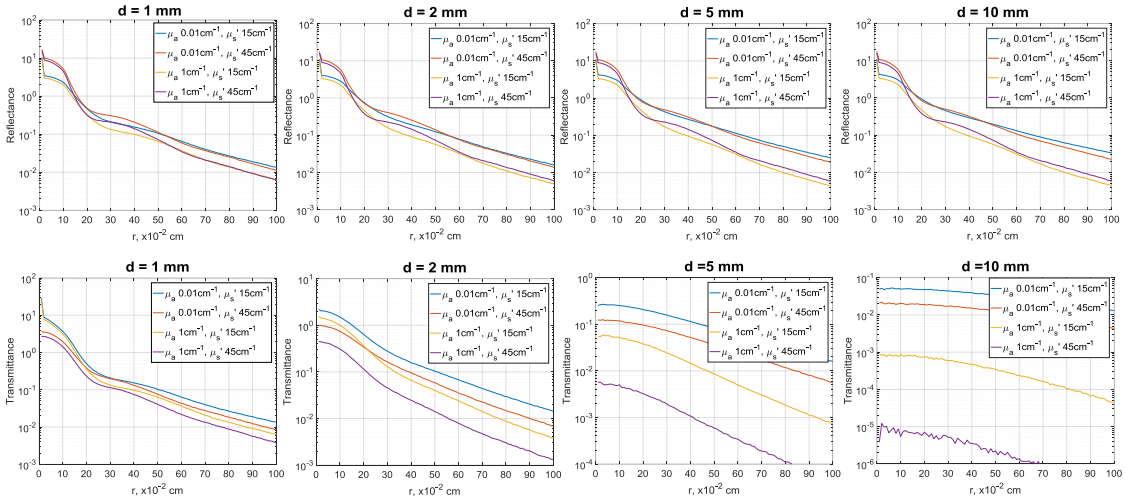

Figure 3. MCML reflectance and transmittance simulated *R(r)* data for various combination of μ_a and μ_s' with different phantom thickness at 1, 2, 5, 10 mm.

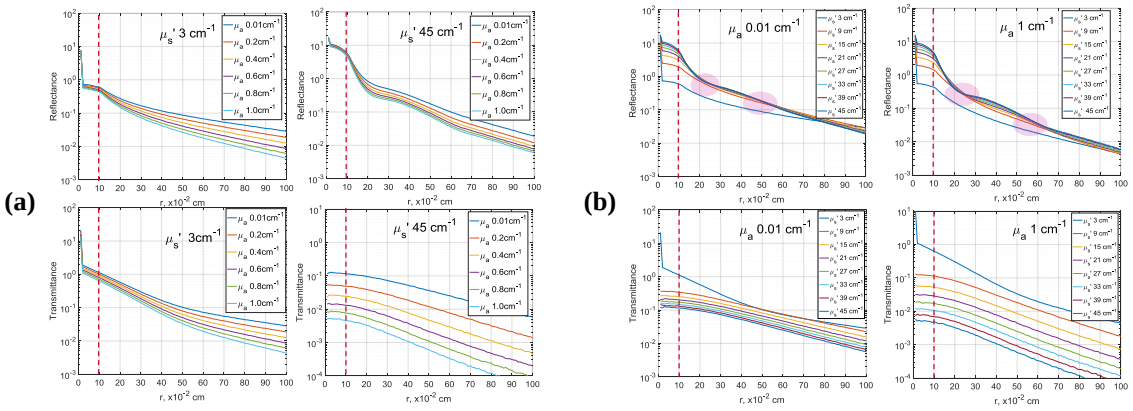

Figure 4. MCML reflectance and transmittance simulated *R(r)* data for various combination of μ_a and μ_s' with phantoms thickness at 5 mm. (a) μ_s' is kept constant at values of 3 and 45 cm^{-1}, respectively, while μ_a varied within the range from 0.01-1 cm^{-1}; (b) μ_a is kept constant at values of 0.01 and 1 cm^{-1}, respectively, whereas μ_s' varied within the range from 3-45 cm^{-1}.

3.2 Phantoms measurement, Calibration model and Forward validation

As previously demonstrated[12, 16], Monte Carlo light-propagation simulation models used in conjunction with multivariate analysis can accurately extract optical properties from reflectance measurement. In this study, multiple polynomial regression (MPR) was employed to create a calibration model to find a mathematical equation of the $R(\mu_a, \mu_s')$ and $T(\mu_a, \mu_s')$ bijective mapping. We chose to calibrate the system on a set of liquid phantoms mixed with milk and India ink. Plots of diffuse reflectance and transmittance at 630 nm as a function of the absorption coefficient μ_a and the scattering coefficient μ_s (logarithmic scale) are shown in figure 5. The dots represent the experiment data of reflectance and transmittance measurements of forty nine liquid phantoms combining the high and low levels of scattering and absorption coefficient. The surface plots represent the curve fitting. The higher-order models although are more accurate in general,

in this case, a third-order model for reflectance and a fourth-order model for transmittance were chosen to compromise the accuracy and robustness for the predictions. The scattering coefficient μ_s was logarithmic scale which gave much more accuracy fitting than linear scale.

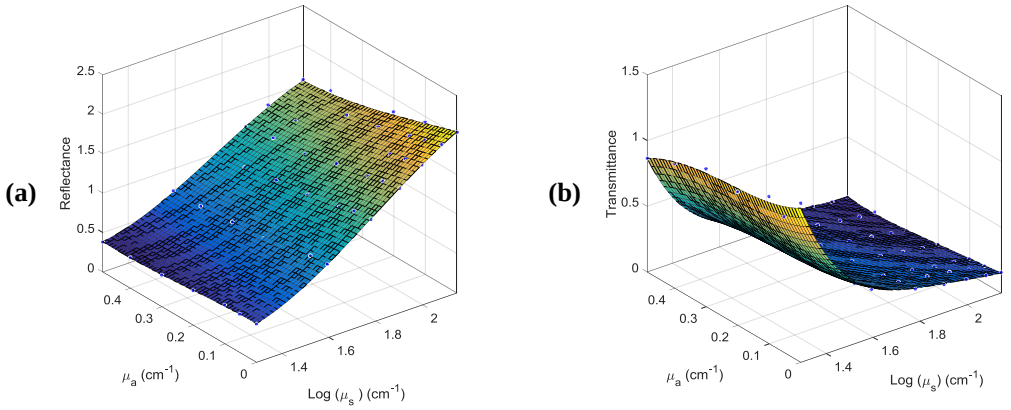

Figure 5. Diffuse reflectance *R* **(a)** and transmittance *T* **(b)** as a function of the absorption coefficient μ_a and the scattering coefficient μ_s (logarithmic scale). The dots represent the experiment data of reflectance and transmittance measurements with a matrix of milk-ink phantoms. The surface plots represent the curve fitting, the reflectance was used a third-order model, while transmittance was used a fourth-order model.

The scatter plots of the measured versus fitted diffuse reflectance and transmittance values from calibration set of liquid phantoms are presented in figure 6(a) and figure 6(b). The red points are nicely distributed on the black lines in both figures, which indicate the acquired third-order model for reflectance and fourth-order model for transmittance fitted the data well. R^2 value and fitted error are 0.9984, 1.70 % for reflectance, whilst 0.9978, 6.45 % for transmittance respectively.

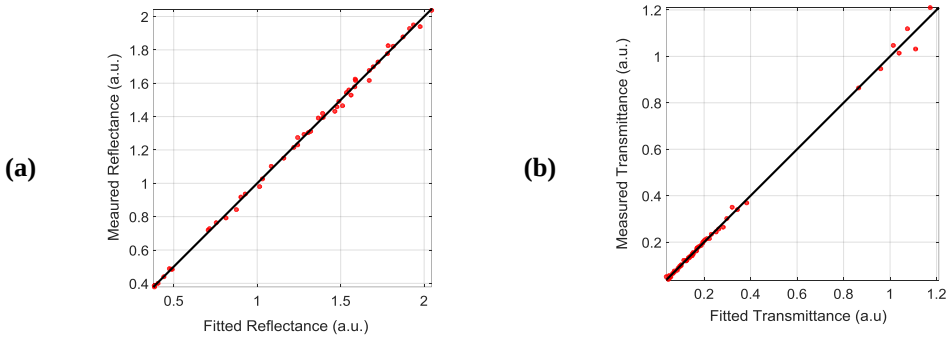

Figure 6. Scatter plots of the measured versus fitted diffuse reflectance **(a)** and transmittance **(b)** for the calibration set of liquid phantoms.

3.3 Prediction algorithm and Inverse validation

A Newton-Raphson algorithm was performed for solving nonlinear equation system and extracting μ_a and μ_s' from the measurements of diffuse reflectance and transmittance. To test the performance of the algorithm, predictions test was performed using the original diffuse reflectance and transmittance measurement data for calibration model as input to extract μ_a and μ_s. The relative predictive errors was calculated as

$$\text{Relative Error } (\%) = \left|\frac{\mu_{pred} - \mu_{ref}}{\mu_{ref}}\right| \times 100 \qquad \textbf{(4)}$$

Where μ_{pred} is the predicted value and μ_{ref} is the true value of either μ_s or μ_a.

Figure 7 shows the predictive error of using Newton-Raphson algorithm to extract μ_s and μ_a from the measurement of diffuse reflectance and transmittance. The average predictive error of μ_s is 1.91 % and μ_a is 7.51 %. The inner matrix of phantoms have lower predictive error.

To further validate the method, we also tested it on reflectance and transmittance data from similar matrix phantoms prepared with mixture of milk-ink. Figure 8 shows correlation plots of actual optical properties versus values predicated by the MPR method from measurements using fibre-optics probe system. It can be seen that the predicted scattering and absorption coefficients of the validation phantoms are correlated well with the expected optical properties with R^2 values of 0.997 and 0.975, respectively.

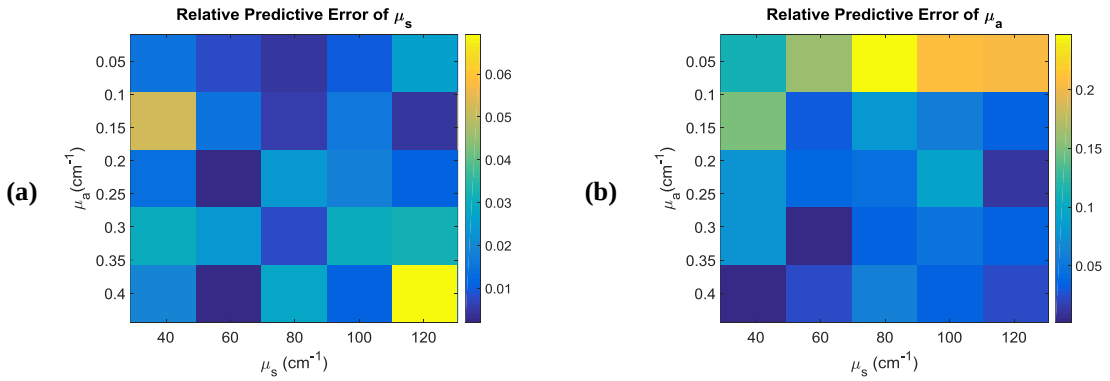

Figure 7. Predictive error of using Newton-Raphson algorithm to extract μ_s **(a)** and μ_a **(b)** from the measurement of diffuse reflectance and transmittance.

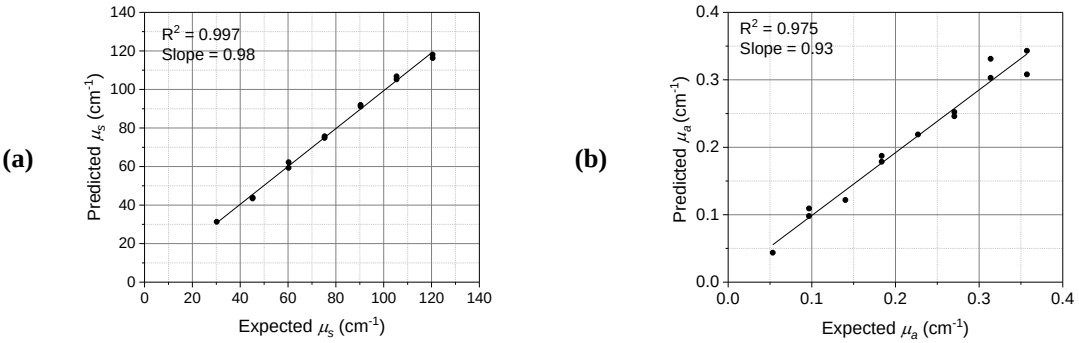

Figure 8. Correlation plots of actual optical properties of μ_s **(a)** and μ_a **(b)** versus the values predicated by the MPR method from phantom measurements.

4. CONCLUSIONS

This paper demonstrated a simple, convenient fibre-optics probe system for the determination optical properties of tissue-like phantoms based on diffuse reflectance and transmittance spectroscopy measurement applicable in small sample volume. Results obtained indicated the general concept is achieved. Further study is required to improve the accuracy of μ_a. Nevertheless, in comparison to other methods, our proposed method is simple, fast and convenient.

The developed system could be used for future real-time determination of optical properties of biological tissue experiment. Furthermore, the measurement data obtained by this approach could be used as an empirical calibration method with a Monte Carlo lookup table-based inverse model for accurate extraction of optical properties from a wide range absorption and scattering coefficients of biological tissue.

ACKNOWLEDGEMENTS

This work is supported by a research grant from the Science Foundation Ireland (SFI) under Grant Number SFI/15/RP/2828. The authors would like to thank Dr. H. Li for the SolidWorks model of cuvette holder and 3D printing.

REFERENCES

[1] Liu, H., Boas, D. A., Zhang, Y., Yodh, A. G., and Chance, B., "Determination of optical properties and blood oxygenation in tissue using continuous NIR light", Phys. Med Biol, 40, 1983 – 1993 (1995).
[2] Nilsson, A. M. K., Berg, R., and Andersson-Engels, S., "Measurements of the optical properties of tissue in conjunction with photodynamic therapy", Appl. Opt., 34(21), 4609 – 4619 (1995).
[3] Cheong, W.-F., Prahl, S.A., and Welch, A. J., "A review of the optical properties of biological tissues", IEEE J. Quantum Electron., 26(13), 2166-2185 (1990).
[4] Jacques, S. L., "Optical properties of biological tissues: a review", Phys. Med., Biol., 58, 37 – 61 (2013).
[5] Pickering, J.W., Prahl, S.A., Wieringen, N. van, Beek, J.F., Sterenborg, H.J., and Gemert, M.J. van, "Double-integrating-sphere system for measuring the optical properties of tissue", Appl. Opt., 32(4), 399-410 (1993).
[6] Thennadil, S.N., and Chen, Y-C., "Alternative measurement configurations for extracting bulk optical properties using an integrating sphere setup", Appl. Spectrosc., 71(2), 224 -237 (2017).
[7] Wilson, B. C., and Jacques, S. L., "Optical reflectance and transmittance of tissues: principles and applications", IEEE J. of Quantum Electron., 26(13), 2186 – 2199 (1990).
[8] Tanaka, K., Tanikawa, Y., Araki, R., Yamada, Y., and Okada, E., "Optical property measurement of thin superficial tissue by using time-resolved spectroscopy", Proc. SPIE 5141, Diagnostic Optical Spectroscopy in Biomedicine II, 315 – 324 (2003).
[9] Fishkin, J. B., Coquoz, O., Anderson, E. R., Brenner, M., and Tromberg, B. J. "Frequency-domain photon migration measurements of normal and malignant tissue optical properties in a human subject", Appl. Opt., 36(1), 10 – 20 (1997).
[10] Alexandrakis., G., Busch, D. R., Faris, G. W., and Patterson, M. S., "Determination of the optical properties of two-layer turbid by use of a frequency-domain hybrid Monte Carlo diffuse model", Appl. Opt., 40(22), 3810 – 3821 (2001).
[11] Yeganeh, H. Z., Toronov, V., Elliott, J. T., Diop, M., Lee, T-Y., and Lawrence K. S., "Broadband continuous-wave technique to measure baseline values and changes in the tissue chromophore concentrations", Biomed. Opt. Express, 3(11), 2762 – 2770 (2012).
[12] Dam, J. S., Pedersen, C. B., Dalgaard, T., Fabricius, P. E., Aruna, P., Andersson-Engels, S., "Fiber-optic probe for non-invasive real-time determination of tissue optical properties at multiple wavelengths", Appl. Opt., 40(7), 1155 – 1164 (2001).
[13] Ninni, P. D., Martelli, F., and Zaccanti, G., "The use of India ink in tissue-simulating phantoms", Opt. Express, 18(26), 26854 – 26865 (2010).
[14] Wang, L. H., Jacques, S. L., Zheng, L. Q., "MCML – Monte Carlo modelling of light transport in multi-layered tissues", Comput. Methods Programs Biomed., 47, 131-146 (1995).
[15] Jääskeläinen, A. J., Peiponen, K.-E., and Räty, J. A., "On reflectometric measurement of a refractive index of milk", J. Dairy Sci. 84, 38 -43 (2001).
[16] Dam, J. S., Dalgaard, T., Fabricius, P. E., and Andersson-Engels, S., "Multiple polynomial regression method for determination of biomedical optical properties from integrating sphere measurements", Appl. Opt., 38(7), 1202-1209 (2000).